LABORATORI NAZIONALI DI FRASCATI
SIS – Pubblicazioni

LNF–99/002 (P)
14 Gennaio 1999

The Local Structure of Ca-Na pyroxenes. II – XANES studies at the Mg and Al K edges

[1)]A. Mottana, [2)]T. Murata, [3)]A. Marcelli, [3,4)]Z.Y. Wu, [3)]G. Cibin, [5)]E. Paris and [5,6)]G. Giuli

[1)]Dipartimento di Scienze Geologiche, Universita' di Roma Tre,
Largo S. Leonardo Murialdo 1, I-00146 Roma, Italy,
[2)]Department of Physics, Kyoto University of Education, 1 Fujinomori-cho,
Fukakusa, Fushimi-ku, Kyoto 612, Japan
[3)]Laboratori Nazionali di Frascati, INFN, Via Enrico Fermi 40, I-00044 Frascati, Italy
[4)]Laboratoire Pierre Süe, Bâtiment 637, CEA-CNRS, CE Saclay,
F-91191 Gif-sur-Yvette Cedex, France
[5)]Dipartimento di Scienze della Terra, Universita' di Camerino, Via Gentile III da Varano, I-62032 Camerino, Italy
[6)]Dipartimento di Scienze della Terra, Universita' di Firenze, Via Giorgio La Pira 4,
I-50121 Firenze, Italy

Abstract

X-ray absorption spectra at the Mg and Al K edges have been recorded on synthetic endmember diopside (Di) and jadeite (Jd) and on a series of natural Fe-poor Ca-Na clinopyroxenes compositionally straddling the Jd-Di join. The spectra of C2/c members of the series (C-omphacites) are different from having P2/n symmetry (P-omphacites). Differences can be explained by theoretical spectra calculated *via* the multiple-scattering formalism on atomic clusters with at least 89 atoms, extending to ca. 0.62 nm away from the Mg viz. Al absorber: XANES detects in these systems medium- rather than short-range order-disorder relationships. Near-edge features of C-omphacites reflect the single-type of octahedral arrangement of the back scattering nearest-neighbours (six O atoms) around the absorber (Mg resp. Al) at the centre of the cluster (site M1). Others arise again from medium-range order. P-omphacites show more complicated spectra than C-omphacites. Their additional features reflect the increased local disorder around the probed atom (Mg resp. Al) induced by the two alternative M1, M11 configurations of the six O atoms forming the first co-ordination spheres. Mg and Al are confirmed to be preferentially partitioned in the M1 resp. M11 site of the P-omphacite crystal structure, however never exclusively, but in a ratio close to 85:15 (±10%) that implies a certain degree of local disorder. Changes in the relative heights of some prominent features are more evident in the Al than in the Mg K-edge spectra. They are diagnostic to qualitatively distinguish C- from P-omphacites.

Key words: diopside; jadeite; omphacite; XAS; synchrotron; magnesium; aluminium

Submitted to Phys. Chem. Mineral.

1 – INTRODUCTION

Ca-Na pyroxenes (Morimoto et al. 1988) have been studied extensively because of the peculiar behaviour of their solid solutions: endmembers crystallise in the C2/c space group, whereas intermediate members can either have the same C2/c space group, or the lower-symmetry P2/n one.

Ordering of the cations located in the octahedral and/or pseudo-cubic sites of the crystal structure has been suggested to be the driving force for such a behaviour (Clark and Papike 1968; Clark et al. 1969; Matsumoto et al. 1975; Curtis et al. 1975; Aldridge et al. 1978; Fleet et al. 1978; Rossi et al. 1981, 1983; Carpenter et al. 1990a,b; and many others; see Mottana et al. 1997a for a referenced review). However, agreement on the actual mechanism that drives the ordering process is far from being reached, in as much as the method chosen to study such an ordering appears to affect the result. As a matter of fact, single-crystal X-ray diffraction structure refinement (SC-XRef), the choice method, gives information mostly on long-range-order (LRO), but it has a bias due to its systematic disregard of vacancies (McCormick 1986; McCormick et al. 1989). On the other hand, Mössbauer spectroscopy (ME) is vastly used to reveal local order in the octahedral site (the one preferred by Fe) and is able to give information also on the little Fe^{2+} that might be located in the pseudo-cubic site. However, it is not effective for Al or Mg i.e., the two predominant cations most likely to be participating in, if not entirely driving the ordering mechanism.

X-ray absorption spectroscopy (XAS) is a technique particularly sensitive to local structure. It is also element-specific, in that it can be modulated at will for any element independently on all others. Therefore XAS can provide new insight into order-disorder (O-D) relationships and local environments across the entire diopside - (omphacite) - jadeite series by selectively scanning either Al or Mg. Information about short-range-order (SRO) gathered by XAS complements that about LRO best obtained by SC-XRef, particularly when near-edge features are being evaluated. Yet X-ray absorption near-edge structure (XANES) spectroscopy has been rarely used, essentially because the absorption K edges of light elements lie outside the range of energies where standard apparatus provides high-quality spectra, and demand for monochromator crystals unavailable till few years ago.

We carried out well-resolved determinations of the Mg and Al K edges in a series of Fe-poor Ca-Na pyroxenes using the most reliable apparatus available at the time. Thus we could provide novel experimental information on Mg-Al ordering in these pyroxenes (Mottana et al. 1996a). However, XANES experimental results could be interpreted properly only by comparison to and with the support of theoretical calculations performed *ab initio* on the basis of the one-electron multiple-scattering theory (MS); in our case starting from crystal structure data determined by SC-XRef.

Elsewhere (Part I: Mottana et al. 1997a), we have reported the results obtained at the Na K edge, and discussed them with reference to our previous studies at the Ca K edge (Davoli et al. 1987; Paris et al. 1995). Thus, we gave complete information on the local structure around the pseudo-cubic site. The aim of this paper is at giving a similar information on the O-D relationships occurring in the octahedrally co-ordinated cation site of the Ca-Na pyroxene structure. There we had been baffled in the past by our inability at measuring atoms other than the heavy ones i.e., Fe and Mn (Davoli et al. 1985, 1988).

2 – STATE OF THE ART

The state of the art about Ca-Na pyroxenes was given in part I (Mottana et al. 1997a) with emphasis on the pseudo-cubic, eight-fold co-ordinated (M2, M21) cation site. We will now enter into details about the octahedral, six-fold co-ordinated (M1, M11) cation site only.

The currently accepted model of the Ca-Na pyroxene structure (mostly after Rossi et al. 1983) is as follows.
(i) Mg and Al are randomly distributed (disordered) over all M1 sites (with point symmetry 2) in C2/c pyroxenes such as diopside (Di) and jadeite (Jd) and the intermediate pyroxenes compositionally closest to these endmembers (C-omphacites). By contrast, they tend to be partitioned (i.e., ordered) over two non-equivalent, very slightly distorted octahedral sites (M1 and M11; again of point symmetry 2) in P2/n pyroxenes of composition near the ratio Di:Jd = 1:1 (P-omphacites). Indeed, in the ideal case Mg and Al would occupy them independently ("full octahedral order"), although not completely, because of the possible concomitant presence in M1 of minor Fe^{2+} and Mn^{2+}, and in M11 of Fe^{3+}, Mn^{3+} and Cr^{3+}. In the real case, Rossi et al. (1983) showed that there is always a certain amount of Mg-Al disorder that increases as the composition deviates from $Di_{50}Jd_{50}$.
(ii) Na and Ca are disordered in the eight-fold co-ordinated M2 site in C-pyroxenes. By contrast, in P-omphacites they are locally ordered over two eight-fold co-ordinated sites (M2 and M21; again with point symmetry 2). The M2 and M21 sites are different in both shape and size. Yet, the Ca and Na atoms are intrinsically disordered over them, despite showing preference to be at least partially partitioned. The degree of this "partial eight-fold site local disorder" is not yet agreed upon, in as much as a further disturbance is the concomitant presence of other cations such as Mn^{2+} and Fe^{2+} (both in minor amounts), plus of vacancies (see above).
Rossi et al. (1983) model is based purely on SC-XRef measurements, and contradicts results of (among others) Clark and Papike (1968), Matsumoto et al. (1975), Curtis et al. (1975) and Fleet et al. (1978). Yet Fleet et al. (1978) had warned against conclusions drawn from SC-XRef evidence only. They claim that the X-ray scattering factors of Mg and Al are very similar and the P2/n structure is not greatly distorted relative to the equivalent C2/c structure. Therefore, the "visibility" of an ordered omphacite is largely associated with the partial order of the M2-type cations i.e., it depends largely on the Na vs. Ca distribution. As a matter of fact, even Rossi et al. (1981 p. 37) had stated that they could only refine the site distribution of Na and Ca between the M2 and M21 sites. By contrast, to determine the populations of the M1 and M11 sites they had to use an indirect, empirical and iterative method combining mean bond distances, charges, number of determined electrons, and with constraints based on the known chemical analysis as well as other basic assumptions.
Later refinements (e.g., Carpenter et al. 1990a; Boffa Ballaran, 1997; Boffa Ballaran et al. 1998a,) significantly improved Rossi's procedure to determine site occupancy, by taking into account a greater number of variables and the sample bulk composition as determined by microprobe. This improved method strongly relies on experimentally determined M-O distances that can be determined by SC-XRef with much greater accuracy than occupancies. Consequently, we know now for sure that in the P-omphacite ideal crystal structure not only Ca and Na are partially ordered, but there is also a degree of Mg-Al ordering with increasing deviation of the sample from the ideal composition, and additionally depends on the sample temperature of equilibration. However, an independent, chemically selective method of determination of the Mg-Al O-D relationships is still opportune, the more so as other cations can compete with Mg and Al in the M1 and M11 sites. Furthermore, SC-XRef is intrinsically suited to provide precise information on LRO, but it deals with SRO only by circumventing numerous difficulties.

Mössbauer spectroscopy (ME) offers such an independent and effective way of determining site occupancy and distribution among sites (SRO as well as LRO), but only for the Fe atom, the amount of which is minor in most Ca-Na pyroxenes. Yet, information on Fe O-D relationships is very important, as this cation may proxy for either Mg or Al depending on its oxidation state. Early ME studies turned out creating interpretation problems rather than

solving them, mainly because of the wrong model assumed for the P-omphacite crystal structure. Later comparative work on both natural and synthetic samples (Dollase and Gustafson 1982), combined with a careful re-interpretation of previous studies (Bancroft et al. 1969; Aldridge et al. 1978), showed that: (a) there is no evidence of Fe^{3+} in any site other than M1 in C-pyroxenes and M11 in P-pyroxenes; (b) the near-neighbour environment of Fe^{2+} is independent on Mg-Al LRO, while size considerations suggest that this cation mostly concentrates in M1 whatever the symmetry is; (c) the occurrence of Fe^{2+} in M2 is not proven, so that the near-neighbour variation model proposed by Aldridge et al. (1978) for P-omphacites needs re-consideration. Electron hopping in neighbouring M1 and M11 sites containing Fe^{2+} and Fe^{3+}, perhaps due to attendant local ordering of Ca and Na in M2, may explain the broadening in the ME doublets of sodic pyroxenes that had been previously interpreted as indicating Fe^{2+} in M2. Note, however, that the presence of some Fe^{2+} in M2 has been independently suggested by SC-XRef (Rossi et al. 1983; Boffa Ballaran et al. 1998a).

Recently, an IR method to determine SRO has been developed (Boffa Ballaran 1997; Boffa Ballaran et al. 1998b) that appears to be able to give information on local structural states down to unit-cell scale. However, as with SC-XRef, IR vibrations depend upon the overall lattice structure, albeit over a smaller distance, so that the IR method cannot provide independent information on the behaviour of selected individual atoms, as XAS and ME instead can do.

3 – XAS SPECTROSCOPY

To the aim of studying short-range-order XAS, a non-destructive technique, is at present the most promising element-specific method. However, XAS studies on Ca-Na pyroxenes are still very limited in number. To our knowledge, there are only a few scattered spectra at the K edge of Al (McKeown et al. 1985: jadeite and glass; Li et al. 1995: omphacite; Li et al. 1996: jadeite glass). Moreover, there is a theoretical study of the Al K edge of jadeite (McKeown 1989): see, in addition, Mottana et al. (1997b, 1998) and Ildefonse et al. (1998). Spectra at the Mg K edge are even fewer (Yoshida et al. 1994: diopside; Ildefonse et al. 1995: diopside and glass; Li et al. 1997: diopside and glass; Cabaret et al. 1998: "diopside", actually a subcalcic augite according to our re-evaluation of their formula). Cabaret et al. (1998) also performed a theoretical simulation of the Mg K edge of diopside. Most spectra had been recorded either to show the potential of the apparatus, or to complete a set of miscellaneous measurements on minerals and/or glasses by giving also the example of a pyroxene. Often, these spectra are so broad and poor in features as to be useless for a systematic crystal chemical study.

The scanty systematic XANES data available on other M1-sited atoms concern Fe only (Davoli et al. 1985, 1988) and are very difficult to interpret. As a matter of fact, omphacite Fe K-edge XANES spectra are broad and unresolved, as they contain contributions from both Fe^{2+} and Fe^{3+}. Therefore, early attempts at quantifying the valence ratio failed (Davoli et al. 1988).

4 – SAMPLES

Two synthetic endmembers, Di and Jd, and nine natural Ca-Na pyroxenes ranging in composition from $Di_{92}Hd_4Ae_3Jd_1$ to $Jd_{94}Di_5Ae_1$ were studied. Four of them had been studied already at the Fe K edge (Davoli et al. 1985, 1988), and seven at the Ca and Na K edges (Davoli et al. 1987; Paris et al. 1995; Mottana et al. 1997a). In addition, we measured a second C2/c Jd-rich omphacite (C.413f: Smith et al. 1980) and a recently characterised P2/n omphacite (70-AM-33: Carpenter et al. 1990a,b; Boffa Ballaran et al. 1998a). Compositional and crystal data for all samples are reported in Table 1 and plotted in Fig. 1.

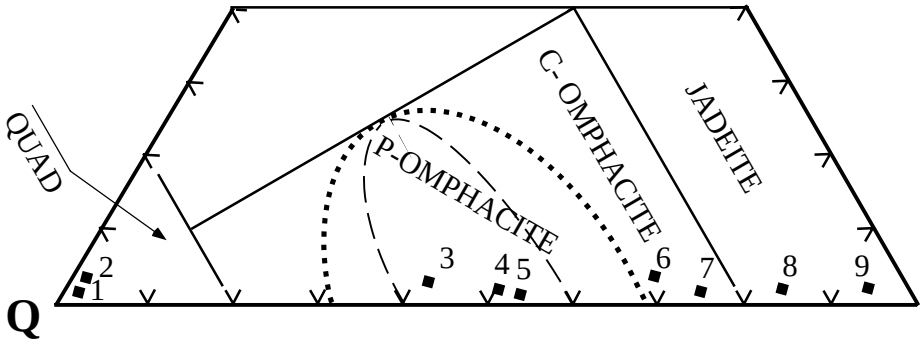

Fig. 1 – Composition of the studied Ca-Na pyroxenes in terms of Jd (jadeite) - Ae (aegirine) - Q (augite) components (Morimoto et al. 1988), after partition of total Fe between Fe^{2+} and Fe^{3+} according to Mottana's (1986) charge balance procedure. Numbers as in Table 1.

Table 1 Chemical and crystal data of the investigated Ca-Na clinopyroxenes (cf. Mottana et al. 1997a, and Fig. 1).

		Components (mol%)			Unit cell data					
		Q	Ae	Jd	a, Å	b, Å	c, Å	dg	V, Å^3	sp.gr.
1	Di	100	0	0	9.748	8.927	5.250	105.83	439.5	n.d.
2	Px-1	98.3	1.7	0	9.750	8.921	5.251	105.81	439.5	C2/c
3	Ala-1	97.3	2.7	0	9.760	8.925	5.258	105.85	440.6	C2/c
4	68-MV-45	55.1	2.3	42.5	9.612	8.794	5.248	106.79	425.5	P2/n
5	M.1	49.8	0	50.2	9.566	8.769	5.252	106.93	421.5	P2/n
6	74-AM-33	47.7	0.4	51.9	9.557	8.752	5.254	106.97	420.3	P2/n
7	C.413f	29.1	5.2	65.7	9.526	8.692	5.246	107.21	414.9	C2/c
8	GR-P1-25	24.4	3.0	72.8	9.510	8.666	5.246	107.31	412.7	C2/c
9	KY#3	15.9	1.2	82.9	9.471	8.608	5.235	107.97	404.9	C2/c
10	MZ	5.2	0.9	93.9	9.439	8.585	5.226	107.46	404.0	C2/c
11	Jd	0	0	100	9.416	8.564	5.226	107.58	401.7	n.d.

1 - Di: endmember diopside, synthetized hydrothermally at 3 kbar, 700˚C, 21 h
2 - Px-1: green diopside in skarn, Canada [incl. SrO 0.035, BaO 0.006, H_2O 0.03]
3 - Ala-1: gem quality colourless "alalite" diopside in rodingite, Val d'Ala, Piemonte, Italy (MMUR 18362/732)
4 - 68-MV-45: dark green omphacite in glaucophane eclogite, Rif. Alpetto, Monviso, Piemonte, Italy
5 - M.1: light green omphacite in vein through metagranite, Lago Mucrone, Biella, Piemonte, Italy
6 - 74-AM-33: pale green omphacite in kyanite eclogite. Munchberg, Bavaria, Germany
7 - C.413f: grass-green omphacite in orthopyroxene eclogite, Nybo, Sorpollen, Norway [incl. NiO 0.02]
8 - GR-P1-25: light green impure jadeite in eclogite, Garnet Ridge, Arizona, U.S.A.
9 - KY#3: white jadeite from jade worker's tomb, Kaminaljuyù, Guatemala (USNM 106443)
10 - MZ: light green jadeite, rough, Manzanal, Motagua valley, Guatemala (USNM 112538-3)
11 - Jd: endmember jadeite, synthetized anhydrously at 30 kbar, 1200˚C, 3 h

All these pyroxenes but three had their structures refined to R = 0.017-0.034 by the late Giuseppe Rossi (pers. comm. 1987) and 74-AM-33 was also solved by the same methods (Carpenter et al. 1990a). Diopside Px-1 was, at Rossi's indication, taken as identical to the Gouverneur diopside (Rossi et al. 1982); by analogy, we considered our natural jadeites to be essentially the same as the Quincinetto jadeite (Rossi et al. 1981). Therefore we used the positional parameters of these two minerals for our calculations. As for our synthetic pyroxenes, we assume, on the basis of the close similarity of the unit-cells, that Di has the same atomic positional parameters as the synthetic diopside refined by Cameron et al. (1973). To our knowledge, no SC-XRef was ever made on a synthetic jadeite (lack of suitable crystals); therefore our Jd was considered at first to be structurally identical to the Santa Rita

jadeite refined by Prewitt and Burnham (1966), then to the New Idria jadeite lately refined by Boffa Ballaran (1997). Both samples, although non-identical, are close to endmember composition.

4.1 – Experimental technique

Information on sample origin, chemical analysis, crystal structure refinement and other physical measurements, as well as on their preparation, was given in Part I. It needs not to be repeated here. However, we add a detailed description of the improvements to the XAS and MS methods specifically introduced for this study.

4.1.1 – XANES spectroscopy

The experimental XANES spectra were collected at UVSOR, the synchrotron radiation (SR) source of Institute of Molecular Science (I.M.S.) at Okazaki, Japan, where the 750 MeV electron storage ring usually operates at 200 mA current with a lifetime of about 4 h (Watanabe 1991). The soft X-ray beamline BL7A derives SR by a super-conducting wiggler under an acceptance angle of 1 mrad in the horizontal plane and of 0.15 mrad in the vertical plane, yielding photons in the energy range 800-4000 eV. The beamline is equipped with a double-crystal monochromator of either beryl or quartz, both crystals being cut along the 100 plane (Murata et al. 1992). Beryl was used to scan across the Mg K edge and quartz the Al one, in both cases by angle steps of 0.01 °ϑ. Resolutions, as determined from the rocking curves, are believed to be better than 1.0 eV for the former crystal, and certainly better than 1.28 eV for the latter one (Krause and Oliver 1979). The sample is spread as a film on a piece of graphite tape, which is adhesive on both sides. The other side of the tape is attached onto the first photocatode of an electron multiplier, which measures the total yield (TEY) of the photoelectrons emitted from the sample by the X-ray excitation as its output current. It is well established that TEY is proportional to absorption taken in the transmission mode (Gudat and Kunz 1977). The entire monochromator plus sample system is held in a vacuum chamber at $1*10^{-7}$ torr.

Table 2 X-ray absorption energies (eV) of the experimental Mg K-edge features of Ca-Na clinopyroxenes.

	A	B	C	D	E	F	G
P1-25	1310.1	1314.0	1318.5	1324.8	1330.7	1345.7	1353.8
C.413f	1310.4	1314.5	1318.9	1326.4	1332.5		
74-AM-33	1310.6	1314.7	1319.2	1326.4	1331.2		
M.1	1310.0	1314.2	1318.7	1325.6	1331.8	1344.2	1353.9
68-MV-45	1310.0	1314.3	1318.7	1325.7	1332.4	1344.5	1354.0
Ala-1	1310.9	1314.6	1319.8	1328.3	1332.5		1351.8
Px-1	1309.9	1314.2	1318.8	1326.2	1330.9	1345.9	1353.7
ΔE	±0.2	±0.2	±0.5	±0.5	±0.5	±0.5	±0.5

Table 3 X-ray absorption energies (eV) of the experimental Al K-edge features of Ca-Na clinopyroxenes.

	A"	A'	A	B	C	D	E	E'	F	G
Jd	1565.1	1566.4	1568.3	1571.7	1576.4	1584.2	1588.9	1593.0	1605.0	1612.6
MZ		1566.0	1568.2	1571.6	1576.3	1584.5	1589.0	1593.6	1604.2	1613.2
KA#3	1565.2	1566.4	1568.2	1571.8	1576.3	1583.8	1588.8	1593.0	1604.1	1613.4
P1-25	1565.2	1566.0	1568.3	1571.8	1576.5		1589.0		1605.5	
C.413f		1566.6	1568.3	1572.4	1576.9	1583.2	1587.0	1592.6		
74-AM-33	1565.1	1566.0	1568.2	1572.0	1576.7	1585.0	1588.3		1605.7	1613.1
M.1		1566.3	1568.1	1572.0	1576.5	1585.0	1588.4		1606.5	1614.3
68-MV-45		1566.3	1568.2	1572.0	1576.4	1585.7	1588.7			
ΔE	±0.2	±0.2	±0.1	±0.1	±0.5	±0.5	±0.5	±0.5	±0.5	±0.5

The observed features were carefully located by first fitting the spectrum with an arctangent to account for the edge jump and then each feature with a gaussian function (Tables 2 and 3). Derivatives were also used, especially for the IMS features.

4.1.2 - MS calculation

Theoretical calculations were carried out at INFN-LNF, Frascati, by means of the CONTINUUM computer code, the formalism developed through the years by C.R. Natoli and his co-workers. Our calculation procedure is based on the one-electron multiple-scattering (MS) theory (Lee and Pendry 1975). It was implemented independently, both computationally and theoretically, by considering multiple-scattering paths for the out-going photoelectrons (Natoli et al. 1980; Natoli and Benfatto 1986; Natoli et al. 1990; Tyson et al. 1992; Wu et al. 1996b; see also Durham et al. 1982; Durham 1988). We make use of Mattheiss' (1964) prescription to construct the total potentials of clusters in the muffin-tin approximation i.e., by superimposing neutral atomic charge densities using the Clementi-Roetti (1974) basis set. Muffin-tin radii are chosen according the criterion of Norman (1974), and a 10% overlap between contiguous spheres is allowed to simulate the ionic bond. We performed the calculations using both the Hedin and Lundqvist (1971) potentials (H-L) and Slater's (1979) energy-independent type of exchange (Xα). Both have been tested repeatedly and proved successful for insulating materials. In the present case, Xα showed best in the high-energy IMS region, because not only reproduces the features but it emphasises the intensities, while H-L tend to flatten everything up due to its imaginary part. Calculations were routinely made at steps of 0.05 Ry (i.e., 0.68 eV), but for the first 10 eV above threshold, where the number of steps was doubled to 0.025 Ry. The calculated values are plotted without accounting for any form of broadening or smoothing.

5 – RESULTS

5.1 –Mg K edge

The experimental XANES spectra of our synthetic Di and of natural diopside Px-1 compare well with those of two synthetic diopsides recorded at UVSOR (Yoshida et al. 1994; Li et al. 1997 Fig. 1A); moreover, they compare reasonably well with that of a synthetic diopside recorded at LURE (Ildefonse et al. 1995 Fig. 2). There is also a good agreement with the spectrum of a natural "diopside" recorded at Super-ACO (Cabaret et al. 1998 Fig. 1), despite the significant difference in composition.

The Px-1 spectrum (Fig. 2, top) shows three major features (A, B, C) in the energy range 1305 to 1325 eV (the full-multiple-scattering region, FMS, of Natoli and Benfatto 1986); the second of these (B) is the main-edge. On the high-energy limb of the third feature (C) a poorly resolved shoulder (C') is noticeable (Table 2). At higher energies (i.e., in the intermediate-multiple-scattering region, IMS, of Natoli and Benfatto 1986), there are four broad bumps (D, E, F, and G); the last one is located close to the very end of the XANES region, which is at 60 eV above threshold (cf. Bianconi 1988). Features A and C are equally high, as in Li et al.'s (1997) spectrum, whereas in Yoshida et al.'s (1994) and Ildefonse et al.'s (1995) spectra feature C is weaker than A (ca. 50 vs. 75, the height of B being taken as 100). Previous studies have shown that the height of peak C would decrease strongly when diopside is measured in the glassy state, and shoulder C' disappear. By comparison, therefore, we infer that our natural diopside Px-1 is in a more ordered state than the synthetic samples recorded by Yoshida et al. (1994) and Ildefonse et al. (1995), and just as ordered as Li et al.'s (1997) synthetic diopside and Cabaret et al.'s (1998) natural subcalcic augite.

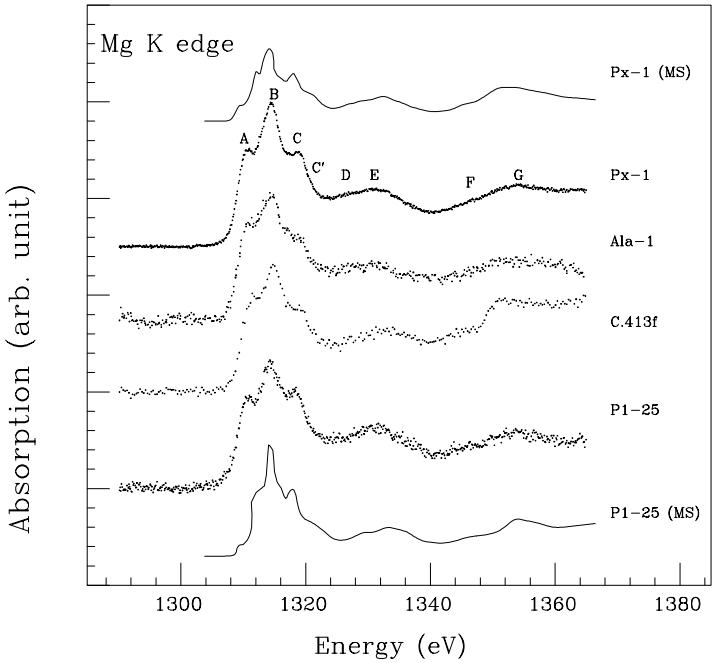

Fig. 2 – Experimental (dotted curve) and MS calculated (continuous curve) XANES spectra at the Mg K edge of C2/c Ca-Na clinopyroxenes of extreme and intermediate composition. Individual spectra have been normalised at the high-energy side (1370 eV) after correcting the base line. See text for explanations.

If this were indeed so, then the somewhat weaker, broader and noisier spectrum recorded for Ala-1 (Fig. 2) would indicate that this diopside is less ordered than Px-1. However, we know that Ala-1 as a bulk sample is compositionally not as homogeneous as Px-1, so that its spectrum too cannot be as well resolved as this one. As a matter of fact, the Ala-1 spectrum is somewhat blurred.

At the Jd-rich end of the compositional join (cf. Fig. 1), C-omphacites C.413f and P1-25 display fairly good XANES spectra (Fig. 2, bottom), albeit with an understandably higher degree of noise owing to their fairly low Mg contents (0.262 resp. 0.204 at.pfu). This also is why the spectrum of KA#3 jadeite (not shown) is poor despite being qualitatively identical to all others. Mg here is such a dilute component (0.113 at.pfu) as to make it surprising that we could even record any spectrum at all when using the TEY technique. Definitively, this was not possible for the MZ jadeite (0.067 Mg at.pfu), the spectrum of which turned out to be flat. KA#3 and MZ bracket compositionally the detection limit for Mg for the X-rays flux delivered by the monochromator of our apparatus.

In spite of these shortcomings, the absorption energies of the Mg XANES spectra for Jd-rich pyroxenes are essentially the same as those of Di-rich pyroxenes (Table 2). This indicates that the arrangement of the six back-scattering O atoms surrounding the Mg absorber does not change substantially when moving from one end to the opposite end of the Di-Jd join. The minor observed energy shifts are to be related to the diminution of the volume of the M1 polyhedron, being Mg now constrained into the space that normally in these compositions would be occupied by Al. However, although not easy to be seen because of the increased noise, the slightly less defined spectrum of P1-25 suggests that this sample has some sort of different Mg ordering than Px-1, or even than the closely related C.413f C-omphacite.

Obviously, this would concern the next-near-neighbour cations of Mg in the M1 strip, since Al is the dominant the nearest-neighbour cation of Mg in this composition.
The energy values of the main absorption features do not change appreciably even when moving across the change in the space group, to P-omphacites (cf. Fig. 2 and Fig. 3; Table 2). Indeed, the major changes we note refer to shoulder C', that disappears altogether, and the noise of the entire spectrum owing to the decreased Mg total content, this noise going hand in hand with lower definition. There is a significant change in the height of main edge B relative to those of features A and C when moving across the entire Di-Jd join. Moreover, feature C independently changes in height also with respect to A, by first becoming weaker, in both C- (Fig. 2, top) and P-pyroxenes (Fig. 3), then turning to be strong again in the C-omphacites closest to the Jd apex (Fig. 2, bottom). As for the IMS region, the P-omphacite spectra appear to contain the same number of features as the C-omphacite ones; actually, D and E are even better resolved despite of the inevitably increased noise. Features F and G are too weak to be significant.

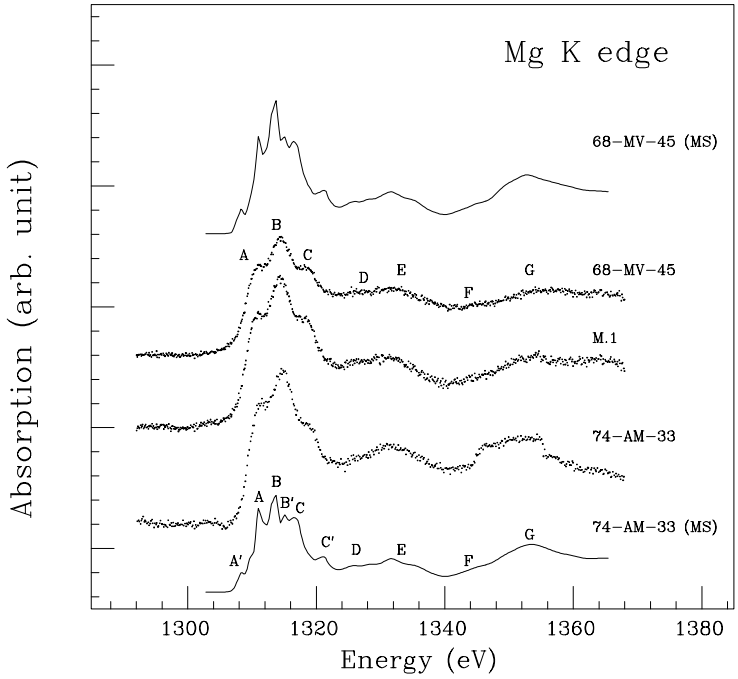

Fig. 3 – Experimental and MS calculated XANES spectra at the Mg K edge of P2/n Ca-Na pyroxenes of omphacite composition. Same conditions as in Fig. 2; see text for explanations.

According to the MS theory, peak intensity is related to the number of MS pathways involving the probed atom and its (first- viz. higher-order) neighbours. Thus, we can anticipate that the presence of either Al or Mg in the neighbouring octahedra of the M1 and M11 strips of P-omphacites certainly affects their Mg K-edge spectra as for peak intensity and definition, although it may not affect them appreciably for their energy. However, in order to interpret properly the observed experimental changes, a comparison with calculated spectra is needed (see below).

5.2 – Al K edge

The experimental XANES spectrum of synthetic jadeite Jd (Fig. 4, top) is fairly similar to that recorded by McKeown et al. (1985 fig. 2), but completely different from Li et al.'s (1996 fig.

4) spectrum. In fact their measured material was not crystalline Jd, rather a high-pressure glass of Jd composition.

The Jd Al K-edge spectrum (Fig. 4) shows five features over the FMS region from 1560 to 1580 eV; furthermore, there are at least three other features, albeit weak, over the IMS region to 1620 eV. A weak shoulder (A") precedes main edge A. It may be interpreted as the pre-peak, and related to violation of the forbidden transitions from 1*s* to empty antibonding *s*-like shells owing to octahedral distortion (Waychunas et al. 1983). Alternatively, it is related to transitions towards Al 3*p* empty states mixed with the empty states of Ca, Na atoms in the nearby M2 site (Wu et al. 1996a). A second, not as strong but well resolved feature (B) follows A, and has two shoulders (C and C') on its higher-energy side. The MZ and KA#3 jadeites have spectra (Fig. 4) which match closely that of synthetic Jd: the only difference lies in the heights of all features, which are lower than the corresponding ones in Jd, but are comparable among the two natural samples. Feature A" is comparatively higher in both of them than in synthetic Jd. In MZ another distinct shoulder (A') occurs on the raising low-energy limb of feature A that was only barely perceptible in the Jd spectrum. This feature may reflect either the high total amount of impurities substituting for Al, or their ordering, because MZ actually contains less impurities than KA#3, where no such feature is visible (0.942 resp. 0.828 Al at.pfu). Definitively, A' is not the pre-peak, but an independent feature arising from structural constraints. Both natural jadeites have their IMS regions less resolved than synthetic Jd, but all four features are present.

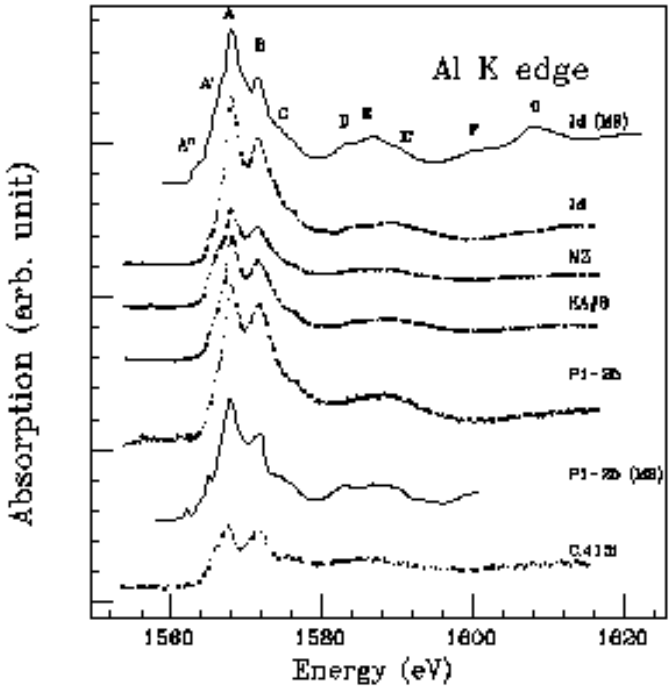

Fig. 4 – Experimental and MS calculated XANES spectra at the Al K edge of C2/c pyroxenes close in composition to the Jd apex of Fig. 1. Individual spectra normalised at the high-energy side (1610 eV) after correcting the base line. See text for explanations.

The experimental Al K-edge spectra of C-omphacites P1-25 and C.413f (Fig. 4, bottom) are almost as strong and well resolved as those of the jadeites in the FMS region, but definitively poorer in the IMS region. They both show a shoulder A' on the low-energy limb of A that is as strong as that occurring in MZ. This supports the inference that it derives from ordering of

the chemical impurities substituting for Al (mainly Mg and Fe^{3+}). In C.413f (and in P1-25 too, but only to a much lesser extent) feature C becomes very weak and another, poorly resolved, but definite feature (C') changes from being a shoulder to become an independent peak. In the IMS region, both spectra consist of two very broad features roughly at the same energies where Jd has E. They are practically flat in the energy range where Jd shows F and G. This is a result of the higher background, which increases in noise owing to the lower and lower Al content (0.705 resp. 0.635 at.pfu). As a matter of fact, diopsides Px-1 and Ala-1, at the opposite end of the Di-Jd join, have an absolutely flat spectrum (not shown) owing to their trifling Al contents.

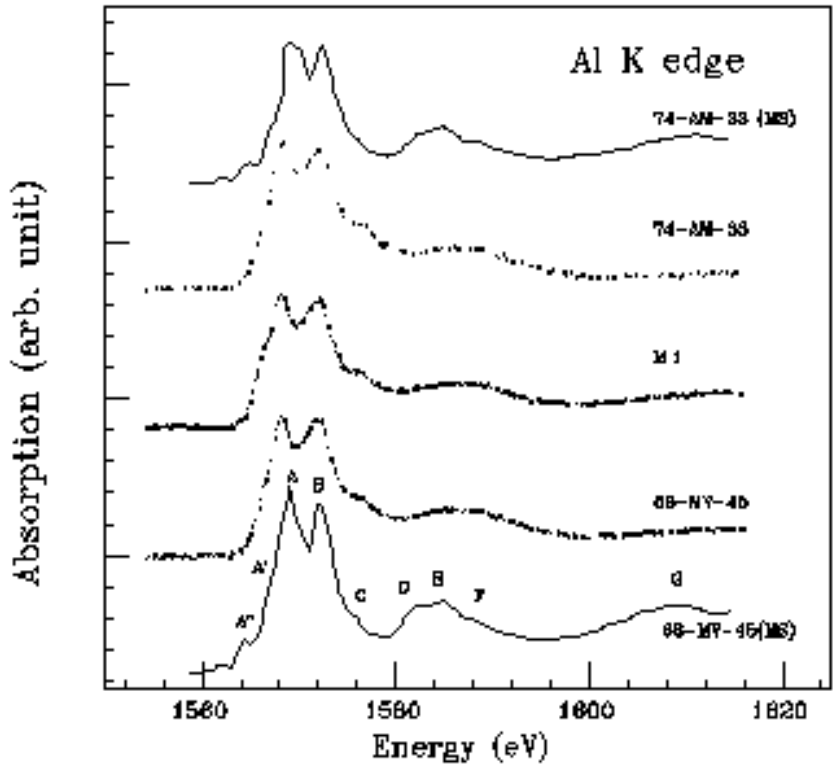

Fig. 5 Experimental and MS calculated XANES spectra at the Al K edge of P2/n Ca-Na pyroxenes of omphacite composition. Same conditions as in Fig. 4; see text for explanations.

Despite of the increased noise, the experimental spectra of P-omphacites (Fig. 5) are resolved well enough as to show a greater number of features than those of C-pyroxenes: note, in particular, the skewed low-energy limb of peak B, which points out for the presence of a unresolved additional feature. Other significant changes to be noted are: (i) A and B have nearly the same height; (ii) A', albeit undoubtedly present, shifts in energy and height to the point of becoming only a vaguely observable shoulder on the low-energy limb of main edge A; (iii) there is no pre-peak A"; and (iv) on the high-energy limb of B, shoulder C not only becomes strong but it also migrates enough to appear as an independent peak (just as in C.413f: cp. Fig. 4). The IMS region consists of only one wide band that encompasses D and E, and is considerably stronger and broader than these were in C-pyroxenes.

All our experimental XANES spectra of P-omphacites appear to be much better resolved than the spectrum of an omphacite of composition $Jd_{53}Di_{44}Hd_3$ recorded by Li et al. (1995 Fig. 3). This spectrum consists of only four features: the pre-peak at 1566.0 eV, the main-edge at 1568.1 eV (labelled peak C in their Table 4), and two other weaker features at 1570 and 1572

eV. The reason for the observed discrepancy is in the composition of that omphacite, which Li et al. themselves points out to be anomalous (1995 p. 439). For the interpretation of the observed features we defer to the discussion that follows.

6 – DISCUSSION

6.1 – Mg K edge

Our Ca-Na pyroxene Mg K-edge XANES spectra are essentially identical to the published spectra of other minerals where Mg is in octahedral co-ordination with O viz. OH (see above, and in addition Wong et al. 1994 Fig. 5: talc and brucite; Wu et al. 1996b Fig. 5: forsterite). However, spectra are completely different and contain much less features than the spectrum of periclase (cf. Rowen et al. 1993; Wong et al. 1994; Ildefonse et al. 1995; Wu et al. 1996b) i.e., the model compound where Mg is indeed in the most regular octahedral co-ordination.

We explain this evidence by taking for granted that XANES displays here one of its best properties: it is able to show how a polyhedron deforms i.e., changes its central angles, even when co-ordination number and bond-lengths remain the same (cf. Bianconi 1988). As a matter of fact, while all compounds listed above have their six Mg-O bonds essentially constant in the range 0.2071~0.2105 nm, their Mg site symmetry lowers from *m3m* for the ideal MgO_6 octahedron of periclase to *-3m* for the $Mg(OH)_6$ polyhedron of brucite, and further lowers to 2 for the MgO_6 octahedron of diopside and to -1 and *m* for the two independent MgO_6 octahedra of forsterite. It finally reaches the 1 and -1 point symmetries for the two highly irregular $MgO_4(OH)_2$ polyhedra of talc. Octahedral quadratic elongation (OQE, cf. Robinson et al. 1971) is an even more convenient measure of polyhedral distortion in that it combines both angle and distance distortions. OQE increases from 1.0000 in periclase to 1.0161 in brucite, and then it drops to 1.0050 in diopside to increase again to 1.0260 resp. 1.0269 in forsterite, and to 1.0086 resp. 1.0087 in talc.

Therefore: a merohedral (lower-symmetry) arrangement of the O nearest-neighbours in the first co-ordination shell appears to generate Mg XANES spectra with a reduced number of features with respect to the holohedral (high-symmetry) arrangement (i.e., the one that occurs in periclase). However, site symmetry is not the unique factor, and OQE, being a function of both distance and angle, better correlates with the overall shape changes of the FMS region of the spectrum. Diopside is typical in this regard: its spectrum resembles those of talc and brucite, rather than forsterite. This happens even though the oxygens co-ordinating Mg in the former minerals are bound to H to form hydroxyls, while in the latter are tied to a divalent cation as in diopside: obviously the binding energy plays a role in this matter.

In order to understand the implication properly, we computed the Mg K-edge spectrum of diopside according to the MS formalism *via* atomic clusters of increasing size up to convergence. Inter-atomic distances and monoclinic 2 point-symmetry were those of the M1 site for all clusters, being Mg constrained only there in the pure synthetic system (Cameron et al. 1973). The calculated spectra converge for clusters containing at least 89 atoms (7 Mg + 10 Ca + 19 Si + 53 O) extending to 0.62 nm away from the Mg atom taken as the absorber.

Our calculated spectrum (Fig. 2, top) broadly agrees with the diopside spectrum calculated by Cabaret et al. (1998 Fig. 1), and represents an improvement over it for the IMS region. Yet, it does not look as good as that, in the FMS region, because we neither convoluted our calculated features with a Lorentzian function nor made use of the Dirac-Hara (D-H) exchange potentials as they did. In MS calculations, convolution (smoothing) of the spectra is optional, but the choice of the potentials is crucial. We decided to stick to Slater's Xα method even after computing our spectra also with the H-L and D-H methods, because the Xα energy-independent potentials permit a better comparison of the calculated spectra between

C- and P-pyroxenes. As a matter of fact, the Xα method emphasises the heights of the D, E, F, and G peaks, while the H-L method exhibits a damping effect after about 10≈15 eV from threshold that makes the calculated IMS spectrum definitively poorer than the experimental one. As for the D-H potentials, apparently they are better suited for the FMS region, but fail to reproduce the IMS region. Cabaret et al.'s and our own calculated FMS spectra have two characteristics in common: (i) features A, B, C and C' are all present and comparable; (ii) there is a small feature (unlabelled) at a energy lower than that of the A feature which does not show up in the experimental spectrum. By contrast, they differ in that: (i) the energy differences among the three major features are not as precisely reproduced by our method as they are by theirs; (ii) their IMS calculated spectra contain only two broad features, against four in ours and in the experimental spectrum.

In detail (Fig. 6, left panel), peaks B and G (and, possibly, D too) already appear in the calculation for a cluster containing only 7 atoms (cf. Wu et al. 1996b Figs. 1 and 2). Therefore, they arise from interaction of the photoelectron emitted by Mg with the six O nearest-neighbours of the first co-ordination shell. These peaks do indeed reflect fundamental atomic properties of the Mg-O interaction and give indication about SRO around Mg at the M1 site of pyroxene. All other features, in particular A and C, arise when the cluster attains a considerable size (ca. 0.60 nm i.e., 50 atoms at least), and match the experimental data when as many as 89 atoms are taken into account over a sphere ca. 0.70 nm in diameter. Thus, they are indicators of medium-range order i.e., they give information about sample crystallinity on a spatial resolution that cannot be attained by SC-XRef yet.

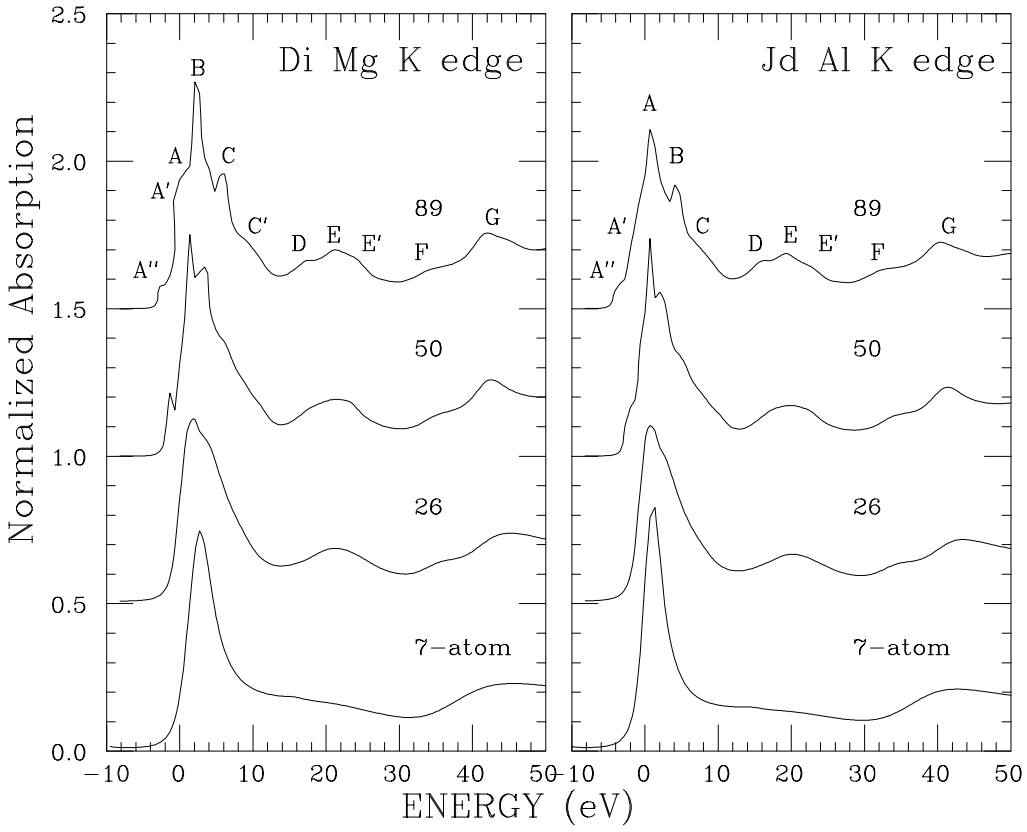

Fig. 6 MS calculated spectra at the Mg (left) and Al (right) K edges in C-pyroxenes Di (synthetic diopside) and Jd (New Idria jadeite) for clusters with increasing number of atoms (indicated on each curve).

The Mg K-edge calculated spectrum of P1-25 C-omphacite (Fig. 2, bottom) is the example for an intermediate Ca-Na clinopyroxene where Mg is diluted and disordered over an M1 octahedral chain occupied mostly by Al. The convergent cluster contains 89 atoms (7 Mg/Al + 10 Ca/Na + 20 Si + 52 O) to 0.62 nm away from the Mg absorber. The spectrum essential features are in good agreement with those just given for Di. However, certain characteristics that made the experimental spectrum of P1-25 remarkable when compared with those of the Di-rich Px-1 and Ala-1 pyroxenes are faithfully reproduced, such as peak C increase in intensity and A drastic decrease. Note that the energy separations between D and E, and between F and G, are easy to be seen in the calculated spectrum while they could not be resolved in the experimental one. From this point of view, an MS calculation that starts from the actual atomic co-ordinates determined by SC-XRef on the sample complements and obviates the poor resolution of its experimental spectrum due the dilution in the structure of the probed atom. Furthermore, calculation makes one aware of the difference in the degree of order existing in the actual sample with respect to the LRO that SC-XRef determines instead and is reflected into the calculated spectrum. As a matter of fact, local disorder or SRO may explain the discrepancies between the P1-25 experimental and calculated spectra (Fig. 2).

Turning now to P-omphacites, in Fig. 3 we plot the calculated spectra for the two compositional extremes, 68-MV-45 and 74-AM-33 (cf. Fig. 1). In these calculations we considered Mg to be fully partitioned in M1, and obtained convergence for clusters containing at least 89 atoms (5 Mg + 2 Al + 6 Ca + 4 Na + 20 Si + 52 O) and extending 0.61~0.62 nm in radius, as in C-pyroxenes. The P-omphacite calculated spectra are very similar to those of C-pyroxenes in their IMS regions (cp. Fig. 2 with Fig. 3) which best reflect the similarity of the overall structure (cf. Aldridge et al. 1978). However, most features appear to be doubled (e.g., D and D’, E and E’) as a result of the increased order of the structure signified by its P2/n space group. Then, local disorder coupled with experimental broadening makes so as to smooth all these features into a broad band although sometimes unequivocal differences may still be detected (Fig. 3). Indeed, where P- and C-pyroxenes differ greatly is in their calculated FMS regions. P-pyroxenes are always considerably richer in features than C-pyroxenes, and show (Fig. 3) at least four main calculated features (A, B, B', C), plus one shoulder (A’) on the raising limb of feature A, located in between A” and A. It is reasonable to surmise that each FMS feature would turn out to be doubled, had calculation been continued to a higher accuracy. Furthermore, note that feature C' at +11 eV, which in C-pyroxenes was only a shoulder, is now a resolved although weak peak; however, this feature cannot be resolved in any experimental spectrum yet.

An increase in the number of calculated FMS features is related to a greater complexity of the electronic transitions around Mg. In experimental spectra, experimental broadening may obliterate such a complexity and force many individual features to merge into few ones. Indeed this is the case with our P-omphacites, where we noted only the three major peaks similar to those occurring in C-pyroxenes, although a little broader and smoother than these. Such calculated features as B' and C merge into a sort of plateau, being resolved enough (thus detectable) only in the M.1 P-omphacite experimental spectrum (Fig. 3). Indeed, to become aware of this problem, and be led therefrom to extract from recorded spectra more precise information about the arrangement of atoms around the probed atom, one must calculate the theoretical spectra. Simulation, combined with a careful evaluation, can better explain variations in the experimental spectra of Ca-Na clinopyroxene than the usual, albeit very carefully applied fingerprinting method.

The M1 site of a P-omphacite differs from that of a C-omphacite in two main points: (i) much greater average size, (ii) greater distortion. E.g., <M1-O> is 0.2068 nm with OQE = 1.0138 in natural 74-AM-33 P-omphacite (cf. Boffa Ballaran et al. 1998 Table 5b); they drop to 0.1999 nm resp. 1.0096 after its annealing at 950 °C, when symmetry turns to C2/c (cf. Boffa

Ballaran et al. 1998 Table 5a). Consequently, we assume that the greater complexity of the calculated FMS regions of our P-omphacites reflects the activation of a number of additional MS paths in their unusually large M1 octahedra; these pathways would overlap with others when activated in a smaller environment such as the M1 octahedron of C-pyroxenes. If this were indeed the case, then any Mg located in the even smaller M11 octahedron of a P-omphacite (see below) would produce a spectrum that does not coincide at all with the M1 spectrum. Such a spectrum may be experimentally detected by subtracting from the total Mg K-edge spectrum the spectrum for Mg in the M1 octahedron of a reference sample e.g., diopside. Nevertheless, to deconvolute the two superimposed spectra a preliminary calculation of both contributions is needed, and a greater resolution in the experimental spectrum than presently possible should be achieved to perform a quantitative evaluation of the data.

6.2 – Al K edge

The calculated Al K-edge spectra of C- and P-pyroxenes display the same major doublet as the experimental ones, but they contain additional information useful to deconvolute them into a considerably greater number of features.

In Jd, the reference example for a disordered C-pyroxene, the calculated spectrum (Fig. 4) indeed consists of at least ten features, among which four in the IMS region which have essentially the same characteristics as those occurring in the IMS region of the calculated Mg spectrum (cp. Fig. 3); however, they are much closer in energy one to the other. Therefrom, we infer the XAS confirmation of what is already well known from SC-XRef i.e., in a jadeite the Al atom distributes over the crystal structure according to the same symmetry rules as Mg in diopside or, in other words, Al occupies in Jd the same M1 sites as Mg in Di, but in a smaller volume (as intrinsic in its smaller ionic radius). In turn, this finding confirms, once more, that the features in the IMS region of a K-edge spectrum arise from contributions of higher order related to the crystallinity of the sample i.e., reflect the same medium- to long-range ordering rules that control SC-XRef. The mean free path of the photoelectron is system-dependent, but on average does not reach 1.0 nm in the IMS region. By contrast in the FMS region the mean free path may be significantly longer (Muller et al. 1982; Bianconi et al. 1987). Therefore, the features in the FMS region are associated to a limited number of MS paths, and it appears that MS calculations require an effort of manipulation of certain critical parameters such as potentials and muffin-tin overlap (10~15%). Nevertheless, calculation is on the right track, and the number of calculated features matching the experimental ones is increasing with time. Unfortunately, contraction due to the small radius of Al affects also this region of the spectrum so that several calculated features in fact are so close as to overlap to a certain extent. They may not be found in the experimental spectrum, where they are further convoluted into few ones because of the resolution. Nevertheless, to the purpose of demonstrating the unique capability of XANES of determining local symmetry around a specified atom, the FMS features are the most significant, albeit still the most difficult-to-interpret piece of evidence.

In order to achieve this goal, in Fig. 6 (right panel) we report the sequence of calculated Al K-edge spectra for Jd obtained with increasing clusters till convergence (i.e., for a cluster of 89 atoms (10 Na + 11 Al + 18 Si + 50 O) extending to 0.61 nm from the absorber). The main edge and feature G are present even in the smallest cluster: they represent interaction between Al and its surrounding shell of 6 O neighbours in the M1 octahedron, as previously described. All other features arise only when next-nearest atom shells are being added to this cluster, and a full agreement between calculation and experiment is never reached for the FMS region, not even when agreement is attained for the IMS region with a cluster containing 89 atoms. We must stress once more our conclusion that the MS theory indeed is on the right track to

decipher the FMS part of the XAS spectrum, but it does not fully simulate it yet. There are still problems in the choice of the parameters. This is why our calculations differ so much from those performed by McKeown (1989 fig. 5b). He thought he could reproduce the jadeite Al K edge with a cluster containing only 9 atoms i.e., three additional atoms beyond the octahedral core, but he did not succeed, as he himself correctly pointed out (McKeown 1989 p. 682).

Therefore, for the time being, we point out that our calculated FMS region of Jd contains the same four features (and pre-peak A") as the corresponding FMS region for Mg in Di. The two FMS spectra differ only in the energy spacing and relative heights of the three major features, in such a way as to make the first feature (labelled A') appear as only a vague shoulder down below the second one (labelled A). This had not been the case in the Mg K-edge spectrum of diopside, where the three major peaks were fairly well resolved (Fig. 6, left). Features are now labelled differently because the present assignment coincides with that in the experimental spectrum, but such a mismatch actually does not exist. Therefore, calculation confirms the expected close similarities of the local arrangements around the probed Mg and Al atoms, and supports the validity of the "fingerprinting" method of XANES evaluation. At the same time, it clarifies that all differences to be seen between the Mg and Al K-edge experimental spectra arise from differences in the average size of the sites, the two atoms being located in sites identical for symmetry. Thus, the problem is brought back to its stereometric essentials.

The Al K-edge calculated spectrum of P1-25 omphacite (Fig. 4) is the example for an intermediate Ca-Na C-pyroxene where Al is indeed the predominant (0.705 at.pfu), but Mg is also significant (0.204 at.pfu) over the M1 octahedral chain. The essential features are in good agreement with those just given for Jd. Note, however, that some more features become apparent that were not so evident in the Jd spectrum. In particular, after features D and E, the IMS region clearly shows the additional feature E'. The presence of this fairly intense E' at a small energy distance from D and E explains well the broad plateau to be seen in this part of the experimental spectrum. Similarly in the FMS region, the small, but resolved calculated feature A' attracts attention on the weak, barely detectable shoulder on the raising slope of the experimental main edge that could otherwise be mistaken for the pre-peak.

Turning now to P-omphacites, in Fig. 5 we plot the calculated Al spectra for the two compositional extremes, 68-MV-45 (0.451 Al at.pfu) and 74-AM-33 (0.256 Al at.pfu; cf. Fig. 1). In these calculations, we considered Al to be fully partitioned in M11, and we obtained convergence for clusters containing 89 atoms, as in C-pyroxenes. The IMS regions of both C- and P-pyroxenes (cp. Fig. 4 with Fig. 5) are very similar, thus confirming the similarity of their structures in the medium-range. By contrast, these P-omphacites differ from C-pyroxenes in their calculated FMS regions, particularly as for the relative width and height of their two major features. These differences are much emphasised in the calculated spectra than they were in the experimental spectra, where experimental broadening and possibly also some local disorder forces certain features to merge. The site where Al preferentially partitions in a P-omphacite is M11, which differs from M1 (i.e., the site where Al is in a C-omphacite of identical composition), for: (i) the much smaller average size, and (ii) the smaller distortion. E.g., in natural 74-AM-33 P-omphacite, <M11-O> is 0.1932 nm and OQE 1.0067 (cf. Boffa Ballaran et al. 1998), as against 0.1999 nm resp. 1.0096 for <M1-O> in the same grain turned to C-symmetry after 458 h of annealing at 950 °C (see above). Consequently, the increased complexity of the Al K-edge calculated spectra may be related to of the Al-O bond, or to superimposition of contributions from two different environments (see below).

7 – COMPARISON BETWEEN K EDGES

A direct comparison between the calculated K edges of Mg in diopside and Al in jadeite (Fig. 6) is the best possible evidence supporting the close similarity of their structural environments through their spectroscopic behaviours. Indeed, the IMS regions of the two convergent clusters display the same sequence of four features with identical shape. Moreover, E' although very weak, may be guessed to be present in both spectra (see above). We already recognised all these IMS effects to be due to medium-range ordering (MRO), since they develop when the clusters attain considerable sizes (at least 0.6 nm). In any case such a distance is much less than the repeat estimated to produce X-ray diffraction. For XRD, at least several unit cells are needed i.e., 2~3 nm. We conclude, therefore, that the IMS region of a XANES spectrum is indeed sensitive to the symmetry induced by the crystalline state of the material as a whole, but over a significantly shorter range (MRO) than SC-XRef (LRO). IMS contains much better indications on local disorder than SC-XRef may ever have. Note, however, that lack of a visible difference between our experimental and calculated spectra may be due to our calculation strategy. The atomic positional data determined by SC-XRef that we used as input for our calculations have errors at the fourth decimal figure of nm. By contrast, in these systems we could prove that our calculations show distinct differences only when atomic displacements are of the order of some thousand of nm. Consequently, some fine details in the XRD information are getting lost in performing calculations. This is a limitation intrinsic in the XAS method that has to be taken into account as long as this procedure is used.

The calculated FMS regions for the Al and Mg K edges appear to differ in their overall appearance (Fig. 6) even when the materials examined turn out to have the same MRO, as inferred from their similar IMS regions. However, this discrepancy is more visual than real (see above).

In diopside, the M1 site occupied by Mg is a fairly regular octahedron (OQE = 1.0050) having three pairs of Mg-O bonds respectively 0.2050(1), 0.2065(3) and 0.2115(1) nm long (Cameron et al. 1973 Table A-7) or, in other words, four nearly equal short bonds and two long ones. In jadeite, the M1 octahedron occupied by Al is less regular (OQE = 1.0152) since all three Al-O bond pairs are substantially different in length, being 0.1995(2), 0.1940(1), and 0.1852(2) nm. Since the local environments are similar, then both the Mg and Al FMS regions are intrinsically structured to show three features, and it is indeed inexplicable why we do not the same neatly separated features for Al as for Mg. We know now that this odd XANES structure is certainly due to a MRO effect, because in all our calculations it shows up for clusters having a large number of atoms (cf. Wu et al. 1996a). We argue that this different spectroscopic behaviour has also something to do with the electrostatic character of the bond. As a matter of fact, Mg-O is definitively ionic, while Al-O has a covalent component that varies among different compounds and may be even rather significant. This is long since known from multiple-scattering self-consistent-field Xα cluster calculations (Tossel 1975) recently confirmed *via* improved theoretical methods (Causa' et al. 1986; Sousa et al. 1992). Consequently, in this system the Mg K edge can be easily reproduced by MS calculations using the CONTINUUM code that had been designed for molecular and ionic substances (Natoli et al. 1980; cf. Tyson et al. 1992). An excellent example for such a calculation is MgO, periclase (Wu et al. 1996b Fig. 1). By contrast, the Al K-edge spectrum could be reproduced only after many attempts: see α-Al_2O_3, corundum (Mottana et al. 1998 Fig. 1).

A final note of warning: both calculated spectra for the 89-atom cluster have distinct pre-edges (A") that do not show up in the experimental spectra.

The close similarity of the Mg and Al K edges of omphacites bears additional evidence to the belief that a XAS spectrum up to about 50 eV from threshold (XANES: cf. Bianconi 1988) mainly depends on the geometrical configuration of the finite cluster of atoms that surrounds

the absorber atom. Then, the interpretation of XANES in terms of full multiple scattering resonances of the photoelectron within a cluster of finite size in the real space is being validated.
However, alternatively, XANES may also be interpreted as the product of the partial density of states and of the matrix element (Bianconi and Marcelli 1992 and references therein). Muller et al. (1982) originally developed this form of explanation. They showed that XANES spectra might be understood as the products of an atomic-like term with a solid-state term. This one contains the projected density of states (DOS) at the photoabsorber site. The DOS approach is equivalent to the MS approach but relates to a different physics. It correlates the overall magnitude and shape of a spectrum to the corresponding atomic transition rate, while its fine structure of is determined by the solid state factor, which is proportional to the density of states according to the dipole selection rule that governs the photoabsorption process. Therefore, the DOS approach makes it clear why the Mg and Al XANES spectra have so many similarities and also so many significant differences; the latter ones occur near the edge, where the projected local and partial density of states is certainly different between the two atoms.

7.1 – Octahedral occupancy

Turning now to P2/n pyroxenes, Fig. 7 shows the calculated spectra for omphacite 68-MV-45 with the Mg (left) and Al (right) absorbers alternatively located at the centre of one of the two different M1 and M11 environments (Na and Ca having been displaced accordingly). We calculated these theoretical spectra for the convergent clusters containing 89 atoms in every case, and with the alternative geometries of each site as determined by SC-XRef. None of the two pairs of calculated spectra closely matches the experimental ones (Fig. 7, middle), either in the FMS or in the IMS region. We will disregard the latter one, because of the spectral noise. The reduced amounts of both Al and Mg in this omphacite and the disorder co-operate to make so that the various features convolute into one or two broad bands. As for the FMS region, in agreement with the current model (cf. Rossi et al. 1983), our calculations favour the general idea that Mg is located in M1 and Al in M11 (see above), but in both cases a certain amount of correction is needed. Indeed, the amount of the observed misfits should be evaluated to the purpose of testing the effect of the local disorder.
The spectrum calculated for Mg constrained in the M11 octahedral site (Fig. 7, left) shows a number of features that are strongly compressed over a small range of energies. This is just the same as Al does when in the M1 environment, however with the characteristic two features still well resolved (Fig. 7, right). Therefore, a two-featured spectrum is confirmed to be typical of Al in octahedral co-ordination, probably because of the covalent character of the Al-O bond (cf. above, and Mottana et al. 1998). This is not so for Mg; yet the M11 Mg spectrum is such as to disprove the possibility that significant Mg may be located in that site. However, the misfit between calculated and experimental Mg K-edge spectra is such as to clearly hint that Mg cannot be all in M1; consequently some of it has to be located in M11. Indeed, misfit is somewhat reduced when the M1 and M11 calculated spectra are superimposed and combined (Fig. 7, bottom left), the most favourable ratio being 85:15. As a confirmation, adding a contribution from the spectrum calculated for Al in the M1 site to that of Al in M11 again in the ratio 15:85 would also improve a little the match with the experimental spectrum (Fig. 7, bottom right) using the same combination ratio. Moreover, the M11+M1 combination makes better sense of feature D and E in the experimental FMS region. Admittedly, our method of esteem of disorder is still rather crude, and in the need of being improved. Yet, XAS confirms that the early axiom about the "full octahedral order" of Mg in M1 and Al in M11 in the P-omphacite structure is untenable, and contributes to this revision by adding chemically selective evidence that is intrinsic in it. The quality of our experimental

spectra is such as to give us little chance at better quantifying the inferred distribution of both Mg and Al over the two sites. Indeed, there are additional reasons for local disorder e.g., the substitutions of other competing cations (albeit minor they may be) such as Mn^{2+} and Fe^{2+} in M1, and Fe^{3+}, Cr, Ti in M11. These substitutions induce a chemical disorder that couples with the broadening of the features due to both the little experimental resolution and the possible interactions with higher-shell cations such as Ca and Na located in M2 and M21. All together they contribute to our still very large degree of uncertainty.

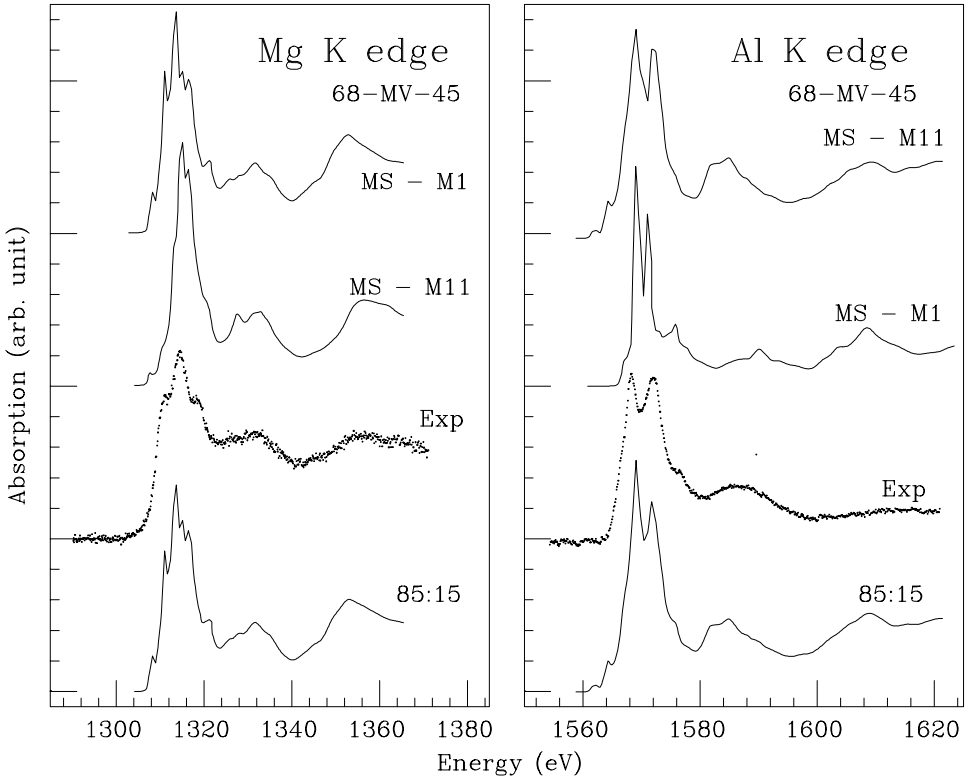

Fig. 7 – MS calculated spectra at the Mg (left) and Al (right) K edges in P-omphacite 68-MV-45 for converging clusters containing 89 atoms, but with different locations of the absorber (two top curves), compared with the experimental spectra (middle dotted curves). The lowest curves are combinations obtained by adding in the 85:15 ratios the calculated spectra above; see text for explanation.

8 – CONCLUSION

The UVSOR wiggler is an intense source, yet it does not induce significant thermal stresses into the monochromator crystals and is exceptionally stable. These intrinsic qualities allow recording at UVSOR soft X-ray spectra at the Mg and Al K edges that display a high degree of accuracy and are worth complete confidence. Consequently, experimental spectra can be evaluated in great detail in spite of their intrinsic experimental broadening. However, successful interpretation is achieved only after theoretical spectra are calculated for the same samples starting from their atomic positional parameters determined by single-crystal X-ray diffraction refinement. These calculated spectra are used for comparison under the assumption that they represent the XANES spectrum of the studied material in the condition of LRO. Differences are then to be interpreted as indicating local deviations from LRO towards MRO and SRO, the evaluation being limited only by experimental broadening and the resolution of the apparatus.

Experimental XANES spectra at the Mg and Al K edges confirm that in all C2/n clinopyroxenes the two atoms occupy M1 sites that are identical in shape. This experimental finding is also supported by MS calculations.
In the UVSOR set-up, the photoelectrons emitted at the Mg and Al K-edge energies probe a volume ca. 0.6 nm in radius. Thus, information on the structure of C- and P-pyroxenes gathered by XAS concerns their medium-range order i.e., has a spatial resolution at least one order of magnitude smaller than that provided by SC-XRef.
C-pyroxenes have the FMS regions of their Mg and Al K-edge spectra that are not as different as they would appear at the first glance. They contain the same number of features, however differently spaced in energy and with different heights so as to show up as three major separated peaks for Mg, and only two major peaks for Al, where the first peak contains two overlapping contributions. The reason for this different behaviour is mainly due to the different degree of ionic vs. covalent character of the Mg-O and Al-O bonds.
The IMS regions of C-pyroxenes are identical for both the Mg and Al K edges, thus implying that the two atoms occupy the same site of the structure (M1) or, conversely, that they are constrained there by the same type of symmetry rules. Since the IMS features arise from interaction of photoelectrons with the higher-order shells of large atomic clusters (at least 89 atoms), this region of the spectrum gives information on medium-range order (MRO) only.
Features in the FMS regions arise from contributions of higher-order shells. Even the white-line contains a large number of MS contributions, although it initially arises from contributions of the nearest six O atoms in the first co-ordination shell.
The IMS regions of P-pyroxenes are essentially the same as those of C-pyroxenes as for their shape, but contain twice as many peaks, suggesting duplication of the periodicity of the atomic array i.e., interaction over a greater volume of the ordered structure.
Calculated features in the FMS region are again twice as many in P- than they are in C-pyroxenes. They reflect the greater complexity of the P-structure even at the local scale, each M1 site being split in two non-equivalent but fairly similar M1 and M11 sites. However, the medium-range well-ordered arrays of Mg and Al remain essentially the same across the C- to P-structure transition. Experimentally, this is better seen in the Al than in the Mg K-edge spectra.
XAS spectra indicate that Mg and Al are not fully partitioned only into the M1 resp. M11 site of the ordered P-structure, as it was often assumed in X-ray diffraction refinement. Comparison with theoretical spectra suggests that, at least in P-omphacite 68-MV-45, partial octahedral occupancies in the 85:15 ratio, such as 0.85 Mg + 0.15 Al in M1 and 0.15 Mg + 0.85 Al in M11, fit the experiments. Thus, although with a large amount of uncertainty (at least 10%), local Mg-Al disorder on a short-range scale exists indeed in P-omphacites, and is here confirmed by an element-selective physical method totally independent upon X-ray diffraction.

9 – ACKNOWLEDGEMENTS

Crystal structure refinements were carried out by the late Giuseppe Rossi (†1987) as a part of a project on alpine omphacites carried out jointly with A.M. that initiated in 1976 and continued till his immature death. M.C. Domeneghetti and T. Boffa Ballaran kindly provided additional information through the courtesy of V. Tazzoli. M. Bondi, L. Morten and D.C. Rubie friendly donated synthetic samples. Natural samples are either our own, or from Museo di Mineralogia della Universita' di Roma (MMUR) and U.S. National Museum (USNM) of Washington D.C., or were received as gifts by those who had studied them. We thank them all. Financial support was granted by M.U.R.S.T., Italy, under Project “Aspetti cristallochimici cinetici e termodinamici”, and by the EU Grant HC&M "Access to Large Facilities". Z.Y.W. acknowledges a temporary contract by the Department of Geological

Sciences of University of Roma Tre during which a number of calculations could be carried out. Experimental work at UVSOR was performed with support from I.M.S. through proposal No. 6-D-567. Discussions and reviews by Rino Natoli, Fritz Seifert, Vittorio Tazzoli and Joe Wong are gratefully acknowledged because they improved significantly the manuscript. Obviously, all remaining errors are entirely our own.

REFERENCES

Aldridge LP, Bancroft GM, Fleet ME, Herzberg CT (1978) Omphacite studies, II. Mössbauer spectra of C2/c and P2/n omphacites. Am Mineral 63: 1107-1115.

Bianconi A (1988) XANES spectroscopy. In: DC Konigsberger & R Prins (eds.): X-ray absorption: principles, applications, techniques of EXAFS, SEXAFS and XANES, pp. 573-662, J. Wiley, New York.

Bianconi A, Marcelli A (1992) Surface XANES. In: RZ Bachrach (ed.): Synchrotron radiation research: advances in surface and interface science, vol. 1, pp. 63-115.

Bianconi A, Di Cicco A, Pavel NV, Benfatto M, Marcelli A, Natoli CR, Pianetta P, Woicik J (1987) Multiple-scattering effects in the K-edge X-ray-absorption near-edge structure of crystalline and amorphous silicon. Phys Rev B 36: 6426-6433.

Boffa Ballaran T (1997) Studio della trasformazione ordine-disordine nelle onfaciti mediante diffrattometria X da cristallo singolo e spettroscopia IR. Tesi Dott Ric Miner Crist IX ciclo, pp. 90.

Boffa Ballaran T, Carpenter MA, Domeneghetti M-C, Tazzoli V (1998a) Structural mechanisms of solid solution and cation ordering in augite-jadeite clinopyroxenes: I. A macroscopic perspective. Am Mineral 83: 419-433.

Boffa Ballaran T, Carpenter MA, Domeneghetti M-C, Salje EKH, Tazzoli V (1998b) Structural mechanisms of solid solution and cation ordering in augite-jadeite clinopyroxenes: I. A microscopic perspective. Am Mineral 83: 434-443.

Cabaret D, Sainctavit P, Ildefonse P, Flank A-M (1998) Full multiple scattering calculations of the X-ray absorption near edge structure at the magnesium K edge in pyroxene. Am Mineral 83: 300-304.

Cameron M, Sueno S, Prewitt CT, Papike JJ (1973) High-temperature crystal chemistry of acmite, diopside, hedenbergite, jadeite, spodumene and ureyite. Am Mineral 58: 594-618.

Carpenter MA, Demeneghetti M-C, Tazzoli V (1990a) Application of Landau theory to cation ordering in omphacite, I: Equilibrium behaviour. Eur J Mineral 2: 7-18.

Carpenter MA, Domeneghetti M-C, Tazzoli V (1990b) Application of Landau theory to cation ordering in omphacite, II: Kinetic behaviour. Eur J Mineral 2: 19-28.

Causa' M, Dovesi R, Pisani C, Roetti C (1986) Electron charge density and electron momentum distribution in magnesium oxide. Acta Cryst B 42: 247-253.

Clark JR, Papike JJ (1968) Crystal-chemical characterization of omphacites. Am Mineral 53: 840-868.

Clark JR, Appleman DE, Papike JJ (1969) Crystal-chemical characterization of pyroxenes based on eight new structure refinements. Mineral Soc Amer Spec Pap 2: 31-50.

Clementi E, Roetti C (1974) Atomic data and nuclear data tables. Vol. 14, No. 3-4. Academic Press, New York.

Curtis L, Gittins J, Kocman V, Rucklidge JC, Hawthorne FC, Ferguson RB (1975) Two crystal structure refinements of a P2/n titanian ferro-omphacite. Can Mineral 13: 62-67.

Davoli I, Paris E, Mottana A (1988) XANES analysis of M1-M2 cations in monoclinic pyroxenes. In: S.S. Augustithis (ed.): Synchrotron Radiation Applications in Mineralogy and Petrology, pp. 97-131, Theophrastus Publ., Athens.

Davoli I, Paris E, Marcelli A, Mottana A (1985) XANES analysis of omphacitic pyroxenes. Terra Cognita 5: 427.

Davoli I, Paris E, Mottana A, Marcelli A (1987) XANES analysis on pyroxenes with different Ca concentration in M2 site. Phys Chem Minerals 14: 21-25.

Dollase WA, Gustafson WI (1982) ^{57}Fe Mössbauer spectral analysis of sodic clinopyroxenes. Am Mineral 67: 311-327.

Durham PJ (1988) X-ray absorption. In: DC Konigsberger & R Prins (eds.): X-ray absorption: principles, applications, techniques of EXAFS, SEXAFS and XANES, pp. 53-84, J. Wiley, New York.

Durham PJ, Pendry JB, Hodges CH (1982) Calculation of X-ray absorption near-edge structure, XANES. Comput Phys Commun 25: 193-205.

Fleet ME, Herzberg CT, Bancroft GM, Aldridge LP (1978) Omphacite studies, I. The P2/n -> C2/c transformation. Am Mineral 63: 1000-1106.

Gudat W, Kunz C (1977) Close similarity between photoelectric yield and photoabsorption spectra in the soft-X-ray range. Phys Rev Letters 29: 169-172.

Hedin L, Lundqvist BI (1971) Explicit local exchange-correlation potentials. J Phys C 4: 2064-2083.

Ildefonse Ph, Calas G, Flank AM, Lagarde P (1995) Low Z elements (Mg, Al, and Si) K-edge X-ray absorption spectroscopy in minerals and disordered systems. Nucl Instr Meth Phys Res B 97: 172-175.

Ildefonse Ph, Cabaret D, Sainctavit Ph, Calas G, Flank AM, Lagarde P (1998) Aluminium X-ray absorption near edge structure in model compounds and earth's surface minerals. Phys Chem Minerals 25: 112-121.

Krause MO, Oliver JH (1979) Natural widths of atomic K and L levels, K· X-ray lines and several KLL Auger lines. J Phys Chem Ref Data 8: 329-338.

Lee PA, Pendry JB (1975) Theory of the extended x-ray absorption fine structure. Phys Rev B 11: 2795-2811.

Li D. Bancroft GM, Fleet ME (1996) Coordination and local structure of Si and Al in silicate glasses: Si and Al K-edge XANES spectroscopy. In: MD Dyar, C McCammon & MW Schaefer (eds.): Mineral spectroscopy: a tribute to Roger G. Burns, pp. 153-163, Geochem Soc Sp Publ 5.

Li D, Murata T, Peng M (1997) Na and Mg K-edge XANES of silicate minerals and glasses. UVSOR Act Report 1996, 202-203.

Li D, Bancroft GM, Fleet ME, Feng XH, Pan Y (1995) Al K-edge spectra of aluminosilicate minerals. Am Mineral 80: 432-440.

Mattheiss L (1964) Energy bands for the iron transition series. Phys Rev A 134: 970.

Matsumoto T, Tokonami M, Morimoto N (1975) The crystal structure of omphacite. Am Mineral 60: 634-641.

McCormick TC (1986) Crystal-chemical aspects of nonstoichiometric pyroxenes. Am Mineral 71: 1434-1140.

McCormick TC, Hazen RM, Angel RJ (1989) Compressibility of omphacite to 60 kbar: role of vacancies. Am Mineral 74: 1287-1292.

McKeown DA (1989) Aluminum X-ray absorption near-edge spectra of some oxide minerals: calculation versus experimental data. Phys Chem Minerals 16: 678-683.

McKeown DA, Waychunas GA, Brown GE (1985) EXAFS study of the coordination environment of aluminum in a series of silica-rich glasses and selected minerals within the Na_2O-Al_2O_3-SiO_2 system. J Non-crystal Solids 74: 349-371.

Morimoto N, Fabriès J, Ferguson AK, Ginzburg IV, Ross M, Seifert FA, Zussman J, Aoki K, Gottardi G (1988) Nomenclature of pyroxenes. Am Mineral 73: 1123-1133.

Mottana A (1986) Crystal-chemical evaluation of garnet and omphacite microprobe analyses: its bearing on the classification of eclogites. Lithos 19: 171-186.

Mottana A, Murata T, Wu ZY, Marcelli A, Paris E (1996) Detection of order-disorder in pyroxenes of the jadeite-diopside series via XAS at the Ca-Na and Mg-Al K edges. J Electron Spectr Rel Phenom 79: 79-82.

Mottana A, Murata T, Wu ZY, Marcelli A, Paris E (1997a) The local structure of Ca-Na pyroxenes. I. XANES study at the Na K-edge. Phys Chem Minerals 24: 500-509.

Mottana A, Robert J-L, Marcelli A, Giuli G, Della Ventura G, Paris E, Wu ZY (1997b) Octahedral versus tetrahedral coordination of Al in synthetic micas determined by XANES. Am Mineral 82: 497-502.

Mottana A, Murata T, Marcelli A, Della Ventura G, Cibin G, Wu ZY, Tessadri R (1998) Characterization of local chemistry and disorder in synthetic and natural α-Al_2O_3 materials by X-ray absorption near edge structure spectroscopy. J Appl Cryst (in press)

Muller JE, Jepsen O, Wilkins JW (1982) X-ray absorption spectra: K-edges of 3d transition metals, L-edges of 3d and 4d metals, and M-edges of palladium. Sol State Commun 42: 365-368.

Murata T, Matsukawa T, Naoe' S, Horigome T, Matsudo O, Watanabe M (1992) Soft x-ray beamline BL7A at the UVSOR. Rev Sci Instrum 63: 1309-1312.

Natoli CR, Benfatto M (1986) A unifying scheme of interpretation of X-ray absorption spectra based on the multiple scattering theory. J Phys C 8, 47: 11-23.

Natoli CR, Misemer DK, Doniach S, Kutzler FW (1980) First-principles calculation of X-ray absorption-edge structure in molecular cluster. Phys Rev B 22: 1104-1108.

Natoli CR, Benfatto M, Brouder C, Ruiz Lopez MZ, Foulis DL (1990) Multichannel multiple-scattering theory with general potentials. Phys Rev B 42: 1944-1968.

Norman JG (1974) Non-empirical versus empirical choices for overlapping-sphere radii ratios in SCF-Xα-SW calculations on ClO_4^- and SO_2. Mol Phys 31: 1191-1198.

Paris E, Wu Z, Mottana A, Marcelli A (1995) Calcium environment in omphacitic pyroxenes: XANES experimental data *versus* one electron multiple scattering calculations. Eur J Mineral 7: 1065-1070.

Prewitt CT, Burnham CW (1966) The crystal structure of jadeite, $NaAlSi_2O_6$. Am Mineral 51: 956-975.

Robinson K, Gibbs GV, Ribbe PH (1971) Quadratic elongation, a quantitative measure of distortion in co-ordination polyhedra. Science 172: 567-570.

Rossi G, Ghose S, Busing WL (1982) Diopside $CaMgSi_2O_6$: refinement of the crystal structure by X-ray and neutron diffraction and preliminary observations on charge density distribution. GSA-MSA Ann Meet Abstr Vol 15, No. 7.

Rossi G, Tazzoli V, Ungaretti L (1981) crystal-chemical studies on sodic clinopyroxenes. In: Rock-forming minerals, pp. 20-45. Proceed XI Gen Meet IMA Novosibirsk, 4-10 Sept 1978.

Rossi G, Smith DC, Ungaretti L, Domeneghetti MC (1983) Crystal-chemistry and cation ordering in the system diopside-jadeite: a detailed study by crystal structure refinement. Contrib Mineral Petrol 83: 247-258.

Slater JC (1979) Quantum theory of molecules and solids. McGraw-Hill, New York.

Smith DC, Mottana A, Rossi G (1980) Crystal-chemistry of a unique jadeite-rich acmite-poor omphacite from the Nybö eclogite pod, Sörpollen, Nordfjord, Norway. Lithos 13: 227-236.

Sousa C, Illas F, Pacchioni G (1993) Can corundum be described as ionic oxide? J Chem Phys 99: 6818-6823.

Tossel JA (1975) The electronic structures of Mg, Al and Si in octahedral coordination with oxygen from SCF-Xα MO calculations. J Amer Chem Soc 97: 4840-4844.

Tyson TA, Hodgson KO, Natoli CR, Benfatto M (1992) General multiple-scattering scheme for the computation and interpretation of X-ray absorption fine structure in atomic clusters with applications to SF_6, $GeCl_4$ and Br_2 molecules. Phys Rev B 46: 5997-6019.

Watanabe M (1991) UVSOR at IMS. Synchr Rad News 4 [3]: 12-17.

Wong J, George GN, Pickering IJ, Rek ZU, Rowen M, Tanaka T, Via GH, DeVries B, Vaughan DEW, Brown GE (1994) New opportunities in XAFS investigation in the 1-2 keV region. Sol State Commun 92: 559-562.

Wu ZY, Marcelli A, Mottana A, Giuli G, Paris E, Seifert F (1996a) Effects of higher-correlation shells in garnets detected by x-ray-absorption spectroscopy at the Al *K* edge. Phys Rev B 54: 2976-2979.

Wu ZY, Mottana A., Marcelli A, Natoli CR, Paris E (1996b) Theoretical analysis of X-ray absorption near-edge structure in forsterite, Mg_2SiO_4-Pbnm, and fayalite, Fe_2SiO_4-Pbnm, at room temperature and extreme conditions. Phys Chem Minerals 23: 193-204.

Yoshida H, Yoshida T, Tanaka T, Funabiki T, Yoshida S, Abe T, Kimura K, Hattori T (1994) Mg K-edge XANES study of silica-magnesia. UVSOR Act Report 1994, 206-207.